Statistical relationship between surface PM 10 concentration and aerosol optical depth over the Sahel as a function of weather type, using neural network methodology

Houda Yahi, Beatrice Marticorena, Sylvie Thiria, B. Chatenet, Catherine Schmechtig, Jean-Louis Rajot, Michel Crépon

Statistical relationship between surface PM_{10} concentration and aerosol optical depth over the Sahel as a function of weather type, using neural network methodology

H. Yahi,[1] B. Marticorena,[1] S. Thiria,[2] B. Chatenet,[1,3] C. Schmechtig,[1] J. L. Rajot,[4] and M. Crepon[2]

Received 10 January 2013; revised 25 October 2013; accepted 27 October 2013; published 12 December 2013.

[1] This work aims at assessing the capability of passive remote-sensed measurements such as aerosol optical depth (AOD) to monitor the surface dust concentration during the dry season in the Sahel region (West Africa). We processed continuous measurements of AODs and surface concentrations for the period (2006–2010) in Banizoumbou (Niger) and Cinzana (Mali). In order to account for the influence of meteorological condition on the relationship between PM10 surface concentration and AOD, we decomposed the mesoscale meteorological fields surrounding the stations into five weather types having similar 3-dimensional atmospheric characteristics. This classification was obtained by a clustering method based on nonlinear artificial neural networks, the so-called self-organizing map. The weather types were identified by processing tridimensional fields of meridional and zonal winds and air temperature obtained from European Centre for Medium-Range Weather Forecasts (ECMWF) model output centered on each measurement station. Five similar weather types have been identified at the two stations. Three of them are associated with the Harmattan flux; the other two correspond to northward inflow of the monsoon flow at the beginning or the end of the dry season. An improved relationship has been found between the surface PM_{10} concentrations and the AOD by using a dedicated statistical relationship for each weather type. The performances of the statistical inversion computed on the test data sets show satisfactory skills for most of the classes, much better than a linear regression. This should permit the inversion of the mineral dust concentration from AODs derived from satellite observations over the Sahel.

Citation: Yahi, H., B. Marticorena, S. Thiria, B. Chatenet, C. Schmechtig, J. L. Rajot, and M. Crepon (2013), Statistical relationship between surface PM_{10} concentration and aerosol optical depth over the Sahel as a function of weather type, using neural network methodology, *J. Geophys. Res. Atmos.*, *118*, 13,265–13,281, doi:10.1002/2013JD019465.

1. Introduction

[2] Desert aerosols are primarily emitted by wind erosion in arid and semiarid regions of the globe. They represent a major fraction of the global emissions of natural aerosols (50% according to *Andreae* [1995] and 37% according to *Ramanathan et al.* [2001]). The north of Africa, including the Sahara desert and the semiarid regions of the Sahel, is considered as the world's largest source of mineral dust [*Prospero et al.*, 2002].

[3] Emissions of desert dust are primarily controlled by meteorological conditions, either directly by the wind velocity or indirectly through the influence of precipitation on soil moisture and vegetation cover [*Brooks and Legrand*, 2000; *Prospero and Nees*, 1977]. For example, a continuous increase in dust atmospheric load has been observed during the periods of drought that occurred during the 1970s to the 1980s, in the Sahel [*N'Tchayi Mbourou et al.*, 1994]. The mineral dust cycle is composed of three phases: emissions from the source areas, atmospheric transport, and deposition. The aerosols are deposited either partly in the generation region or outside, during the transport phase in which they can be advected several thousand kilometers away from their sources. Because of their relatively short lifetime and the geographic location of sources, desert aerosols are heterogeneously distributed [*Andreae et al.*, 1996], inducing a strong variability of their effects. In North Africa, desert aerosols are an important source of nuisance due to huge reductions of visibility during dust storms that impact aerial and terrestrial transport [e.g., *Pauley et al.*, 1996] and air quality [e.g., *De Longueville et al.*, 2009]. In the Sahel, mineral dust is suspected to play a role in the occurrence of meningitis epidemics in the Sahelian "Meningitis Belt". *Thomson et al.* [2006] suggest, for example, that excess dust in late autumn, prior to the seasonal peak of meningitis, may increase its incidence and could have a predictive value for epidemic forecast.

[1]LISA, Universités Paris Est-Paris Diderot-Paris 7, CNRS, Créteil, France.
[2]LOCEAN, Universités Pierre et Marie Curie, CNRS, IRD, Paris, France.
[3]IRD/UJF-Grenoble 1, Dakar, Senegal.
[4]IRD-UMR 211 Bioemco, Niamey, Niger.

Corresponding author: H. Yahi, LISA, Universités Paris Est-Paris Diderot-Paris 7, CNRS, Créteil, France. (Houda.Yahi@lisa.u-pec.fr)

2169-897X/13/10.1002/2013JD019465

[4] The evaluation of the different impacts of desert aerosols requires the quantification of the atmospheric dust content especially near the source areas. Such quantification requires taking into account the strong variability of the dust atmospheric contents induced by weather conditions which affect emissions, transport, and deposition of these aerosols. The variability of desert aerosol atmospheric content can be documented and analyzed by in situ observations, remote sensing, and modeling approaches.

[5] Remote-sensing techniques allow documenting the atmospheric dust load over a large spatial and temporal scale. However, up to now, retrieving aerosol content over bright land surfaces is challenging. Over the arid and semiarid regions of West Africa, the information available from spaceborne remote-sensing techniques was limited until recently, to semi-quantitative indicators such as the absorbing aerosol index (AAI) initially developed for observations from the Total Ozone Mapping Spectrometers [*Herman et al*., 1997; *Torres et al*., 1998] and now available from the recent Ozone Monitoring Instrument observations, or those such as the infrared different dust index (IDDI) derived from Meteosat observations [*Legrand et al*., 2001]. The AAI is known to be sensitive to the aerosol layer altitude [*Torres et al*. 1998; *Hsu et al*., 2004] while the IDDI is sensitive to the variability of the water vapor content during the composition period. More recently, *Hsu et al*. [2004, 2006] developed an algorithm to derive the AOD (atmospheric optical depth) at 490 nm from Moderate Resolution Imaging Spectroradiometer measurements, the so-called deep blue AOD. Comparisons with ground-based AOD measurements reveal a regional dependence in the performance of the "deep blue AOD" with significant variations in the slopes of the regression between the retrieved and measured AOD [*Shi et al*., 2011].

[6] AOD retrieval over land has also been developed, taking advantage of the multiangle viewing capability of the Multiangle Imaging Spectrometer (MISR) instrument and specifically validated over desert locations. But, because of a limited swath width, MISR data do not provide daily coverage on a continental scale. Ground-based remote sensing by Sun photometers gives access to the columnar extinction of solar radiation by atmospheric aerosol: the aerosol optical depth (AOD). The Aerosol Robotic Network (AERONET), a Sun photometer network (http://aeronet.gsfc.nasa.gov/, provides near-real-time observations of the aerosol spectral optical depth and sky radiance and derived parameters such as particle size distributions, single-scattering albedo, and complex refractive index in several stations. Since 1994, 14 stations have been installed in West Africa by the PHOTONS component of the AERONET network, with different periods and durations of observations. They have made it possible to establish the seasonal cycle of the AOD in different stations of West Africa [*Holben et al*., 2001; *Ogunjobi et al*., 2008]. Whatever the technique, i.e., spaceborne or ground-based observations, aerosol indexes or AOD retrievals provide a measurement or a proxy of the total column atmospheric dust load. As a result, for some applications, such as the evaluation of desert dust impact on air quality and health, using the AOD as a proxy of the surface concentration may be a critical issue.

[7] Moreover, an analysis of the variability of the atmospheric dust content based on the AOD can mask some variability due to the altitude of the dust transport.

[8] Typically, in the Sahara and Sahelian regions in summer, mineral dust emitted from the Sahara is transported across the North Atlantic Ocean above the Marine Boundary Layer within the elevated Saharan Air Layer (SAL), as shown by *Prospero and Carlson* [1972] and further supported by lidar measurements performed offshore western Africa [*Karyampoudi et al*., 1999; *Immler and Schrems*, 2002] and on the West African coast [*Léon et al*., 2009]. In Senegal on the northwest African coast from January 2006 to September 2008, the maximum AOD was observed in summer and corresponded to a maximum in the top altitude of the dusty SAL between 2 and 6 km [*Léon et al*., 2009]. An additional low-level layer of increasing depth was observed from late summer to fall. Severe dust storms are systematically observed in spring (March) but with a lower vertical development (maximum extinction below 1.5 km) and a stronger impact on the ground-level mass compared to summer [*Léon et al*., 2009]. Similar trends were evidenced over the African continent using 3 year measurements of the Cloud-Aerosol Lidar with Orthogonal Polarization instrument on board the CALIPSO satellite [*Cavalieri et al*., 2010]. From 2006 to 2008, analysis of lidar profiles overpassing the stations of Banizoumbou (Niger) and Cinzana (Mali) showed the succession of low dust layers (below 3 km) from November to March and elevated ($>$3 km) dust layers from May to October. Apart from this typical seasonal contrast in the altitude of the Saharan dust plumes between summer and winter, almost nothing is known about the variability at the intraseasonal scale, and in particular during the dry season (October–May), where surface concentrations are the highest. Because of this variability in the altitude of the dust layers, the relationship between the surface concentrations and the AOD is not obvious and may depend on the location and on the meteorological context.

[9] The objective of the present work is to study the mesoscale meteorological field (~500 km) surrounding two stations during the Sahelian dry season, the most critical period for health impact studies, and to determine its influence on the relationship between the surface concentrations and the AOD for desert aerosols through the use of statistical methods.

[10] Establishing a relationship between aerosol surface concentrations and AOD relevant in a large variety of situations is a difficult task for several reasons [*Yahi et al*., 2011]:

[11] 1. The sensitivity of the relationship to meteorological conditions,

[12] 2. The different spatial and temporal sampling for AOD and surface concentrations, and

[13] 3. The fact that remotely sensed measurement of AOD yields an integrated quantity for the whole atmospheric column whereas the surface concentration is measured close to the ground level.

[14] In order to investigate the influence of meteorological conditions on the relationship between dust surface concentration and AOD, our strategy was to decompose the mesoscale meteorological situations into a reduced number of weather types [*Brissoli et al.*, 2001; *Vautard et al.*, 1990]. For each of the identified weather type, the relationship between dust surface concentration and AOD was investigated. To perform this statistical analysis, a homogeneous data set of observations and output of a numerical weather prediction model analysis has been set up for the dry seasons from 2006 to 2010. In particular, we used time series of aerosol surface concentrations recorded at two Sahelian stations, namely Banizoumbou (Niger) and

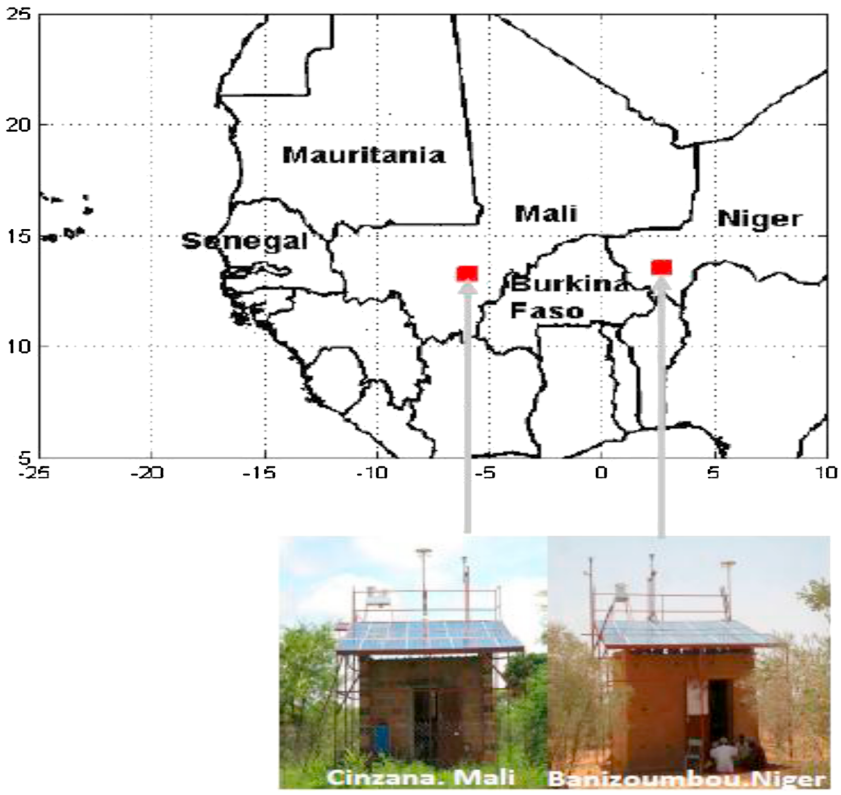

Figure 1. Location of the two experimental sites over West Africa and views of the aerosol sampling stations of Banizoumbou (Niger) and Cinzana (Mali).

Cinzana (Mali) deployed in the framework of the African Monsoon Multidisciplinary Analysis (AMMA) International Program. The paper is articulated as follows: Section 2 presents the database of ground observations and meteorological fields. Section 3 describes the methodology employed to define the weather types, the results obtained during the 2006–2010 dry seasons, and a discussion on the validity of the classification in terms of atmospheric processes. Section 4 analyzes the results provided by the decomposition in classes and studies the seasonal and interannual variability of the data set. Section 5 presents the relationships between the AOD and the surface concentrations estimated for the different weather types and a statistical retrieval of the surface dust concentrations from the AOD measurements. The last section is devoted to a summary of the results and a conclusion.

2. The Data

[15] The geophysical data set used for the statistical analysis gathers different parameters which were measured at regional and local scales. Three kinds of data were used: meteorological fields from the European Center from Medium-Range Weather Forecast (ECMWF), in situ meteorology, aerosol concentration, and AOD measurements.

2.1. In Situ Measurements

[16] In the present study, we used in situ measurements of surface concentration and AOD from two of the three stations of the so-called Sahelian Dust Transect [*Marticorena et al.*, 2010]: the stations of Cinzana (Mali, 13.28N, 5.93W) and Banizoumbou (Niger, 13.54N, 2.66E) (Figure 1). This network was deployed in the frame of the AMMA (African Monsoon Multidisciplinary Analysis) International program and has been fully operational since January 2006. The third station of this network (M'Bour, Senegal) was excluded from the analysis due to a lower recovery rate of the surface concentrations and also because of its localization on the Atlantic coast that induces peculiar local meteorological conditions. The instrumentation of the stations is fully described in *Marticorena et al.* [2010] and briefly reminded hereafter.

2.1.1. Aerosol Surface Concentrations

[17] Atmospheric concentrations of particulate matter smaller than 10 μm (PM_{10}) were measured using a Tapered Element Oscillating Microbalance (1400A from Thermo Scientific) equipped with a PM_{10} inlet [*Yahi et al.*, 2011]. This instrument allows the measurement of particulate concentrations ranging from a few micrograms to a few grams per cubic meters. It has been shown that this instrument is able to provide relevant measurements with a limited cost in terms of maintenance. In terms of sensitivity, the detection limit of the instrument is about 0.06 $\mu g/m^3$ for an hourly sampling time. For the two stations, all measurements have a nominal data acquisition time of 5 min. The annual recovery rate for PM_{10} concentrations ranges between 92 and 99% for the two stations. In the present study, hourly mean concentrations have been computed from the 5 min measurements. For the selected period (dry seasons, i.e., October to May 2006 to 2010), our data set includes 10,825 hourly data for Banizoumbou (Niger) and 10,208 for Cinzana (Mali).

2.1.2. AERONET Ground-Based Measurements

[18] The stations of Banizoumbou and Cinzana are equipped with a Cimel Sun photometer from the AERONET/PHOTONS

network (http://aeronet.gsfc.nasa.gov/). A full description of the instrument and the retrieval procedure can be found in *Holben et al*. [1998].

[19] The aerosol optical depth (AOD) quantifies the extinction due to aerosol integrated over the whole atmospheric column. According to *Holben et al*. [2001], the uncertainty on the AOD retrieved from AERONET Sun photometers on the field is mainly due to calibration uncertainties, which were estimated between 0.01 and 0.02, depending on the wavelength. AERONET Sun photometers are equipped with different channels allowing computing the spectral dependence of the AOD, i.e., the Angström exponent α. This spectral dependence is sensitive to the aerosol size. Desert dust is characterized by micron and super micron particle size modes and thus exhibits very low α (close to 0), while α values higher than 1 are observed when the aerosol mass size distribution is dominated by submicron particles [*Holben et al*., 2001].

[20] For the two stations, we used the level 2 (quality controlled) AOD measurements, automatically made between 05 h and 18 h at three different wavelengths (430 nm, 760 nm, 870 nm). From the individual measurements, we computed 2989 hourly means for Banizoumbou (Niger) and 2294 for Cinzana (Mali) at the three wavelengths during the observation period (dry seasons 2006–2010).

2.2. Meteorological Fields

[21] In this work, we use the meteorological fields provided by the ECMWF analyses obtained by integrating the T106L31 model for the period 2006 to 2010. We extracted 3-D fields of air temperature (T) and meridian and zonal (U, V) wind components at nine pressure levels (1000, 925, 850, 700, 500, 400, 300, 250, 200 hPa), at a spatial resolution of 0.5° over the selected domain (5°N–25°N and 25°W–10°E) with a 3 h time step (00.00, 03.00, 06.00, 09.00,12.00 ,15.00, 18.00, and 21.00 UTC). For the five dry seasons of the years 2006 to 2010 (October to May), this corresponds to 9727 3-D meteorological fields.

3. Methodology

[22] For each station, we have classified the 3-D meteorological fields into a limited number of categories, the so-called weather types. This classification clusters the similarities in the 3-D meteorological parameters in a mesoscale domain (450 km × 450 km) centered at each station. For each weather type, the relationship between the PM_{10} concentration and the AOD is expected to be simplified since the variability of the meteorological field is reduced and consequently its impact on the PM_{10}-AOD relationship. The methodology is detailed in *Yahi et al*. [2011].

[23] The 9727 meteorological fields corresponding to the dry seasons from 2006 to 2010 have been clustered into a huge number of prototypal meteorological situations by using a self-organizing map (SOM). This number was reduced by using a hierarchical ascendant classification (HAC).

[24] SOM is an unsupervised classification method made of a competitive neural network structured in two layers [*Kohonen*, 2001] suitable for clustering large data set, denoted L in the following. The first layer (or input layer) receives the data (here the meteorological fields). The second one is a two-dimensional (10×10 in the present case) neuron grid. Each neuron of the grid captures data of L which are similar. The neuron grid summarizes the information contained in the multivariate learning set D (D being the 9727 meteorological situations). Each neuron j is associated with a referent vector W_j ($0 < j \leq 100$) that has the dimension of the data and is statistically representative of L. The neuron grid presents a topological ordering, which means that similar situations of L are mapped onto neighbor regions on the SOM map, while dissimilar patterns are mapped further apart. The number of neurons (100 here) determines the granularity of the mapping, which in turn is responsible for the accuracy and the generalization capabilities of the SOM map. The reference vectors W_j are determined from L, through a learning process [*Kohonen*, 2001], by minimizing a nonlinear cost function.

[25] The large number of subsets provided by the SOM map permits to take into account the complexity of the input data set. However, it may prevent the synthesizing of some meteorological information embedded in L. To counteract this difficulty, this large number of subsets is aggregated into a smaller number of categories based on the similarities of the subsets. We extracted a few pertinent "weather types" from the subsets by clustering subsets having similar statistical properties, expecting that the "weather types" can be associated with common meteorological characteristics. For that, we used a hierarchical ascendant classification [HAC; *Jain and Dubes*, 1988] using the Ward distance for the intraclass similarities. We aggregated the 10×10 neurons into five statistically significant types. The number of types has been selected choosing the most significant discriminative partition with respect to the dendrogram (or hierarchical tree) of the HAC.

[26] Technically, for each station (Banizoumbou and Cinzana), we applied the SOM algorithm to the vectors representative of meteorological situations (vertical profiles of temperature, zonal, and meridional wind components). The problem was to characterize the input vector of SOM that represents a meteorological situation. The desert aerosols do not only depend on the local meteorological situation but also on the mesoscale meteorological situation, i.e., scales are of several hundred kilometers. In the present study, we have considered that pertinent mesoscale meteorological information is embedded in an area of 450 km × 450 km ((A2) area in Figure 2) centered on the ground stations (Cinzana and Banizoumbou).

[27] For that purpose, we subsampled the 3-D meteorological fields on 17 grid points around the stations (blue cells in Figure 2, and the two red cells correspond to the location of the two stations).

[28] These seventeen cells allowed us to take into account the local as well as the mesoscale weather situations, (the nine cells around ground stations). Each input vector of the meteorological map is thus composed of three vertical profiles of atmospheric parameters (temperature, meridional, and zonal wind components at nine vertical levels) at each of the seventeen grid meshes (Figure 2). The 459 ($9 \times 3 \times 17$) components of the input vector of SOM are output of ECMWF forecast model analysis. Following *Yahi et al*. [2011], we decided to fix the SOM dimension to 10×10, providing a highly discriminating representation of the learning set, L. The learning set was thus clustered into 100 subsets. At each of the two stations, the SOM algorithm was applied to the meteorological data set to produce a two-dimensional

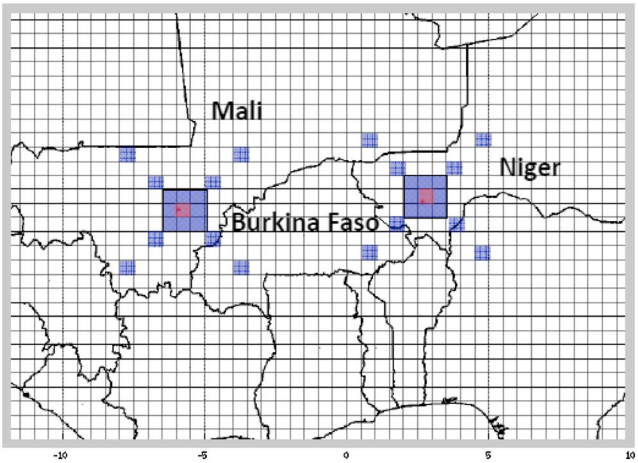

Figure 2. Representation of the grid mesh of the ECMWF atmospheric model and the specific meshes (blue squares) used for determining the weather types at the two stations. The large red squares correspond to the Cinzana and Banizoumbou areas where we studied the profiles of temperature, meridional, and zonal wind components.

SOM map (denoted SOM-B for Banizoumbou (Niger) station and SOM-C for Cinzana (Mali) station) with 10×10 neurons providing 100 typical meteorological situations representative of the five dry seasons 2006–2010 periods. This initial classification was then reduced into a limited number of groups using a hierarchical ascendant classification (HAC) (see Figure 3). The number of groups, or weather types, was selected choosing the most significant discriminative partition with respect to the dendrogram of the HAC, which is the highest level of significantly different classes' distributions at the significance level of 95% using a Kolmogorov test [*Saporta*, 1990]. This test was applied at each significant cutting level of the dendrogram defined by the "rule of the elbow", corresponding to the levels where there is a significant change of the aggregation index, based on the intraclass variance with the Ward distance metric. Five different weather types were finally selected for each station.

4. Analysis of the Classification in Weather Types

4.1. Seasonal Variability

[29] For the two stations, the statistical analysis of the atmospheric fields, done by processing the meteorological data set from the ECMWF on a mesoscale domain surrounding the stations, (Figure 2) leads to the identification of five weather types. These weather types are denoted WTBX (X = 1…5) for Banizoumbou and WTCX (X = 1…5) for Cinzana. At each of the two stations, the five weather types differ both in terms of atmospheric fields of temperature and wind at different levels.

[30] The Sahel is characterized by the succession of two contrasted weather regimes: the Harmattan, characterized by northeasterly flow, mostly blows during the winter and defines the dry season, while in summer, due to the northward

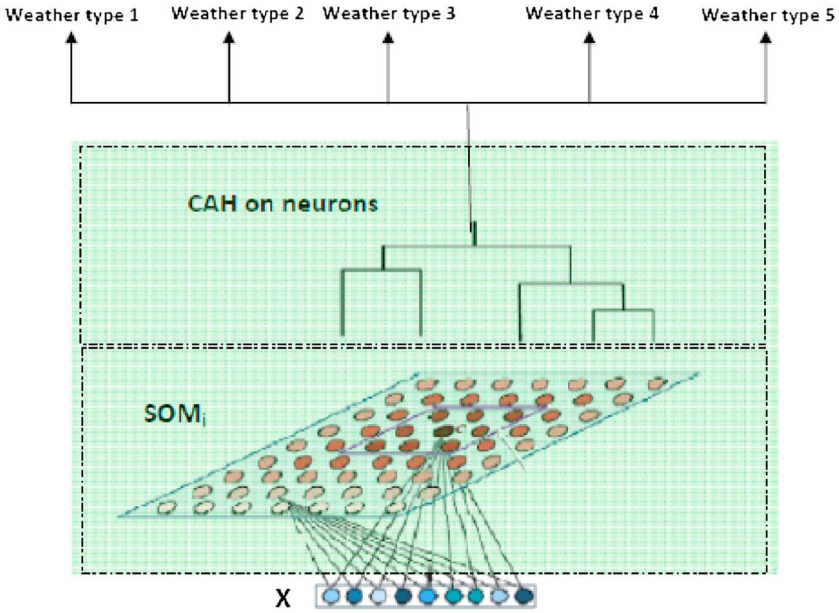

Figure 3. Schematic representation of the method and the structure of the SOM$_i$ map ($i = 1$ for Banizoumbou, Niger, and $i = 2$ for Cinzana, Cinzana). The network comprises two layers: an input layer used to present the observations and an adaptation layer for which a neighborhood constrains is defined (distance d between neurons and a neighborhood function). Each input vector (X) of SOM$_i$ is thus constituted by 17 vertical profiles of atmospheric parameters (temperature, meridional, and zonal wind components at nine vertical levels) at each of the17 grid meshes (Figure 2). The 459 ($9 \times 3 \times 17$) components of the input vector of SOM$_i$ are output of the ECMWF forecast model analysis. Each neuron i of the map is fully connected to the input layer. It is associated with a group that is represented by a reference vector rv which is represented by the weights of the connection to the input layer. The neurons are clustered in classes by a hierarchical ascendant classification.

Table 1. Characteristic of the Weather Types for Each Station From the Observations

Weather Types	Temperature at 2 m (°C)	Mean Wind Speed (m/s) at 10 m	Mean Wind Direction (°) at 10 m
	Station of Banizoumbou (Niger)		
WTB1	32	2.06	230
WTB2	31	0.58	118
WTB3	29	2.08	68
WTB4	25	4.27	61
WTB5	24	3.52	31
	Station of Cinzana (Mali)		
WTC1	31	1.27	212
WTC2	28	1.54	76
WTC3	26	2.4	67
WTC4	24	3.2	40
WTC5	26.5	2	21

displacement of the Intertropical Convergence Zone, the Sahel is exposed to the southwest moist flow of the African monsoon. Moist convection that develops in this monsoon flow provides most of the precipitation in the Sahel [*Mathon et al.*, 2002]. The rainy season associated with the African monsoon lasts from May to October [*Lebel and Ali*, 2009]. In Banizoumbou and Cinzana, the precipitations are much less frequent and intense in May and October, which mostly corresponds to transition periods characterized by the passage of the intertropical discontinuity (discontinuity between the Harmattan and the monsoon flows at the ground level). In this study focused on the so-called dry season, we have selected the period between October and May that includes the core of the dry season (November to March) and the transition periods (April, May, and October) between the Harmattan and the monsoon regimes. The weather types identified are thus expected to be mainly associated with the Harmattan regime. This is confirmed by inspecting the wind direction and the temperature at the ground level determined from the ECMWF meteorological fields. In Banizoumbou, three weather types (WTB3, WTB4, and WTB5) are characterized by east-northeast surface winds, i.e., wind sectors typically associated with the Harmattan flow. Weather types WTB4 and WTB5, respectively, correspond to high-mean wind velocities (4.27 and 3.52 m s^{-1}) (Table 1). They are associated with lower surface temperatures (25°C and 24°C) compared to the southern weather types (32°C and 31°C). Weather type WTB3 exhibits an intermediate temperature (29°C) and a lower wind velocity, which could indicate a transition between the south weather types WTB1 and WTB2 associated with wind directions corresponding to the monsoon flow. WTB1 corresponds to moderate (2.06 m/s) west-southwest winds (230°) and to the highest mean temperature (32°C) among the five weather types. WTB2 corresponds to east-southeast winds (110°) but with very low wind velocity (0.58 m/s) and a slightly lower temperature (31°C) than for WTB1.

[31] The different weather types also differ by their occurrence time during the dry season. Figure 4 presents the average relative monthly occurrence of each weather type at the two stations for the five dry seasons studied. This figure highlights typical temporal patterns in the succession of the weather types during the dry season. As summarized in Table 2, in Banizoumbou, the first two weather types of the two stations (WTB1 and WTB2) are more frequently recorded at the end (May) and the beginning of the dry season (October). The last three weather types (WTB3, WTB4, WTB5) mainly occur in the core of the dry season (from November to March): WTB4 is mainly observed in December (28%), WTB5 in January (34%), and WTB3 in March (23%) (Table 2).

[32] In Cinzana, weather type WTC1 corresponds to a south-southwest wind (212°) and to the highest mean temperature (31°C) among the five weather types (Table 1). The four other weather types are characterized by northeast surface winds.

[33] Weather types WTC2 and WTC3 correspond to the east-northeast winds. They are associated with intermediate surface temperatures (28°C and 26°C).

[34] Weather type WTC2 exhibits an intermediate temperature (28°C) and a lower wind velocity, which could indicate a transition between the south weather types WTC1 and the three other weather types.

[35] Weather types WTC4 and WTC5 respectively correspond to mean wind velocities (3.2 and 2. m s^{-1}) (Table 1). They are

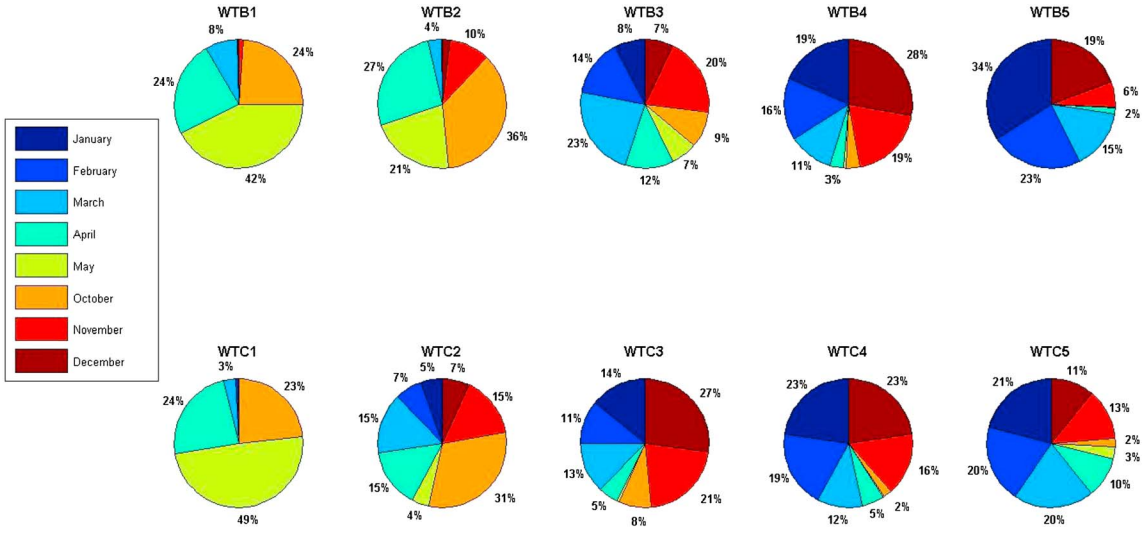

Figure 4. Percentage occupied by the months of the dry season (October to May) for each weather type. Each weather type is represented by a pie chart (see the color legend representing each month).

Table 2. Percentage of Occurrence of Each Weather Type in Winter (November to March) and Months of Maximum Occurrence of Each Weather Type and Their Associated Percentage (See Figure 4)

	Banizoumbou		Cinzana	
	Percentage of Occurrence in Winter	Month of Maximum Occurrence and Percentage of Occurrence (%)	Percentage of Occurrence in Winter	Month of Maximum Occurrence and Percentage of Occurrence (%)
WTX1	9	May (42)	3	May (49)
WTX2	15	October (36)	49	October (36)
WTX3	72	March (23)	86	December (27)
WTX4	84	December (28)	93	December (23)
WTX5	97	January (34)	85	January (21)

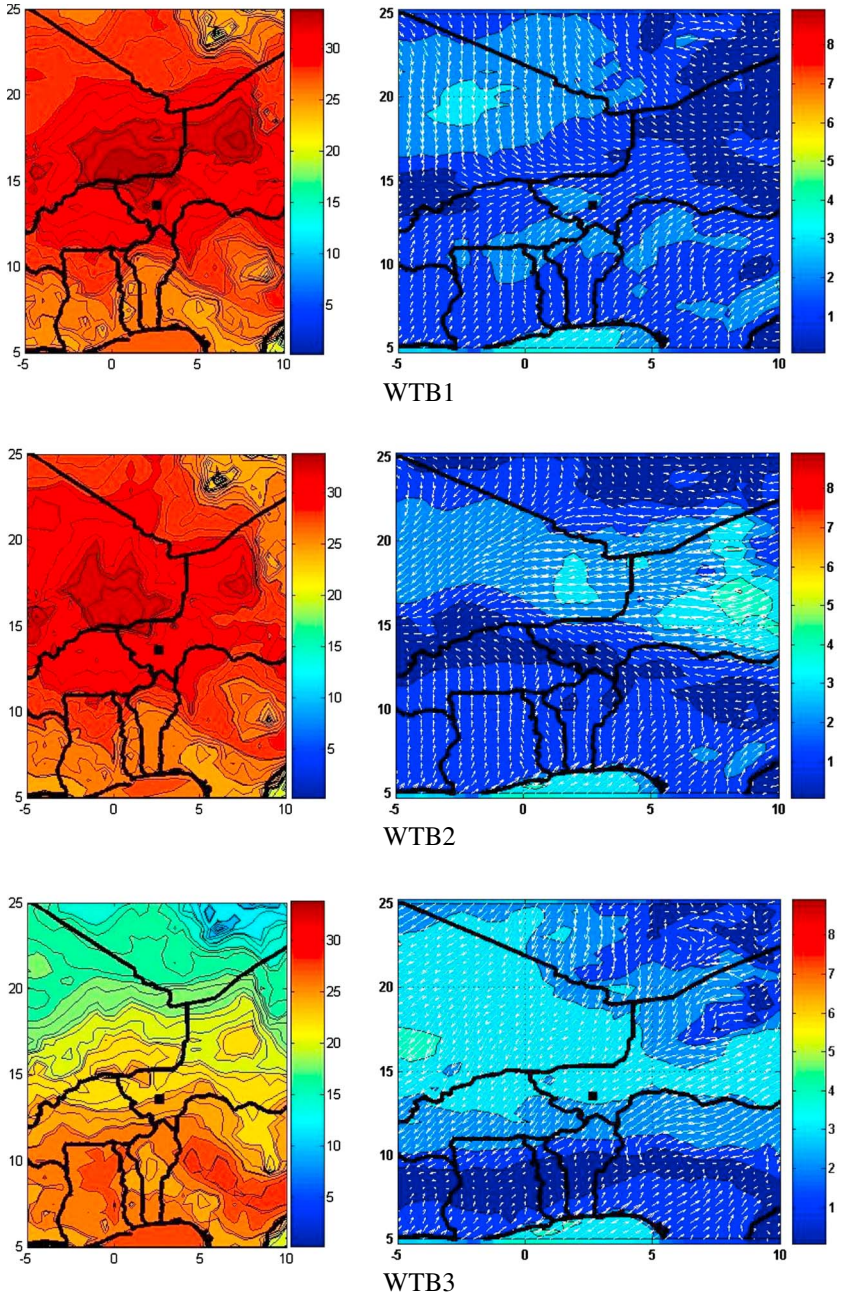

Figure 5. Mean (left) temperature and (right) wind maps obtained in the Banizoumbou (Niger) area at the ground level for the five weather types. The colors indicate the wind and temperature intensity (see the scale at the right of the cartoons).

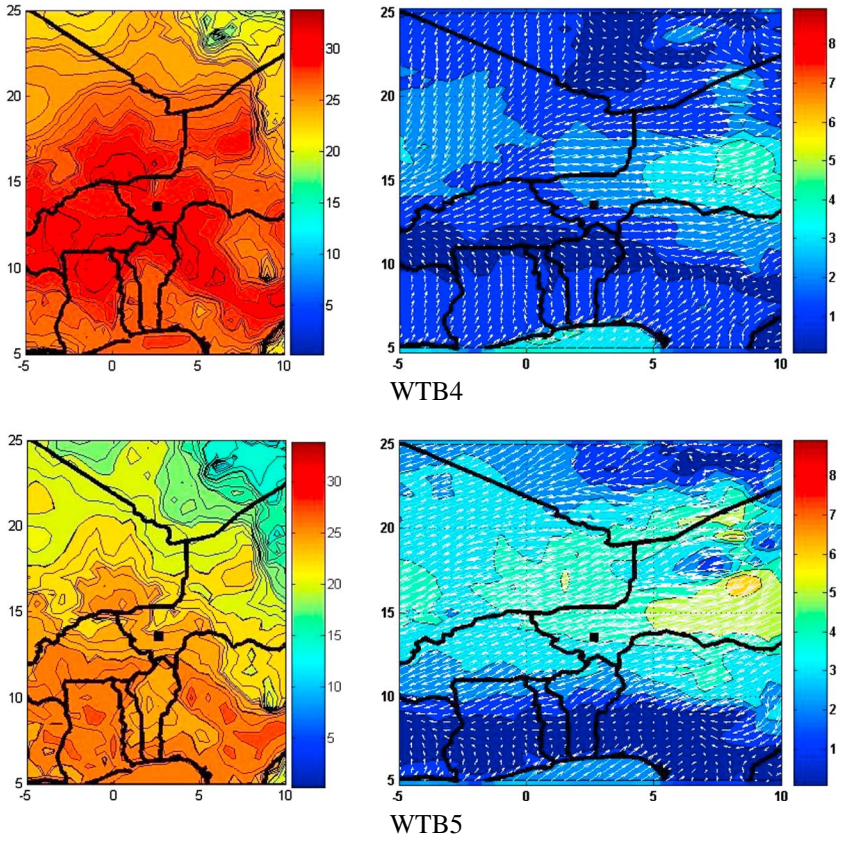

Figure 5. (continued)

associated with lower surface temperatures (24°C and 26.5°C) compared to the southern weather types WTC1 (31°C).

[36] The different weather types at Cinzana have a similar occurrence time during the dry season and comparable percentage of occurrence as the weather types in Banizoumbou (Table 2). The highest occurrence for WTC1 is in May and for WTC2 in October. The three Harmattan weather types (WTC3, WTC4, and WTC5) mainly occur between December and March (Figure 4): 62% of WTC3 situations are observed between November and January, with a maximum in December (Table 1). WTC4 is mainly observed between December and February (65%), with a maximum occurrence in December and January (23% each). WTC5 is observed between January and March, with a similar occurrence during these three months (21 to 20%).

[37] Based on their respective timing and main characteristics, the three Harmattan weather types identified in Cinzana can thus be paired with those observed in Banizoumbou: WTB3 and WTC3 are the main weather time at the beginning of the dry season, i.e., from November to January. Then WTB4 and WTC4 become dominant, while WTB5 and WTC5 are the major weather types occurring in the core of the dry season (from January to March). A general temporal frame of these weather types can thus be established on the intraseasonal scale, with some overlap between the periods of occurrence of the different weather types: the WTB2 and WTC2 mainly occur in October, corresponding to the transition from the monsoon to the Harmattan regime. Once the Harmattan regime is installed, WTB3 and WTC3 dominate during the first phase of the dry season (November–December) before it is progressively replaced by WTB4/WTC4 (December to February), and then by WTB5/WTC5 (January to March). The end of the dry season is characterized by the northward progression of the monsoon flow. WTB1 and WTC1 become progressively dominant from April to May.

[38] For each station, the weather types also differ in terms of mesoscale pattern, as illustrated by the map of mean mesoscale fields of surface winds and temperatures presented in Figure 5 for Banizoumbou and Figure 6 for Cinzana. The three weather types associated with the Harmattan flow in Banizoumbou are characterized by similar spatial surface wind patterns (Figure 5) but with significant differences in mean wind intensity. The intensity of the surface winds in the domain studied (Figure 5) decreases from WTB3 to WTB5 and WTB4. WTB4 is associated with the highest surface winds, which are located south of the Aïr Mountain, in the westward path of the Bodélé Depression region (Chad), known as the most active dust source of the Sahara [*Prospero et al.*, 2002; *Washington et al.*, 2006]. Assuming that the surface wind minimum and the shift from southwest to northeast in the direction of the surface winds permit to locate the intertropical discontinuity (ITD; *Flamant et al.*, 2007), it appears that the ITD occupies a northernmost position for WTB3 than for WTB5 and WTB4 (Figure 5). For these three Harmattan weather types, the Banizoumbou station is located at the northern edge of a zone of high temperature, whose maximum is situated south of 10°N, corresponding to a temperature gradient between the gulf of Guinea and the Sahel which is typical of the transition between the Harmattan and the monsoon flow. Further analysis at the

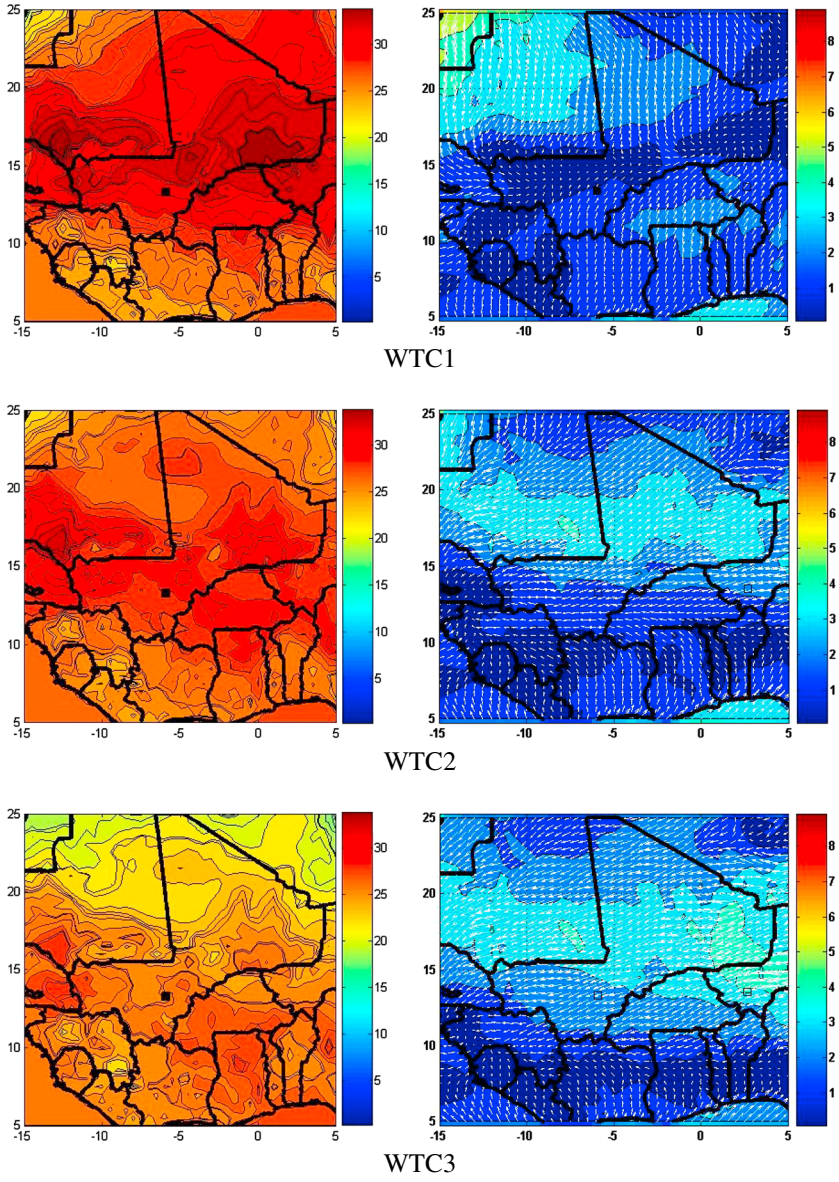

Figure 6. Mean (left) temperature and (right) wind maps obtained in the Cinzana (Mali) area at the ground level for the fives weather types. The colors indicate the wind and temperature intensity (see the scale at the right of the cartoons).

synoptic scale would be required to fully understand the meteorological context leading to these different weather types inside the Harmattan regime.

[39] At the end and also at the beginning of the dry season (May and October), a region of high temperature is observed, with two local maxima, respectively, located around 15°N–17°N and 2°W–4°E and around 16°N–18°N and 6°E–8°E, the station of Banizoumbou being located at the southern edge of this high-temperature area (Figure 5). The location of this high-surface temperature zone and the period of its occurrence suggest that WTB1 and WBT2 are associated with the West African Heat Low (WAHL). Indeed, the climatology (1984–2001) of the WAHL shows that in May, the core of the WAHL is located south of the Aïr Mountain (18°30N and 8°30N; *Lavaysse et al.*, 2010). It is associated with a weak Harmattan flow allowing the monsoon flow to progress northward over the continent especially in May [*Lavaysse et al.*, 2010]. During the wet season, the WAHL moves toward the Sahara (and is thus referred to as the Saharan Heat Low). In October, the maximum of the WAHL takes a position similar to that observed in May, i.e., southwest of the Aïr Mountain before moving eastward to reach the southwest of the Darfur (Sudan). The displacement of the WAHL at the beginning and at the end of the dry season seems connected to the displacement (incursion or retreat) of the monsoon flow over the north of Niger and Mali, reflected by the WTX1 and WTX2. For WTB1, the station of Banizoumbou seems to be located south of the ITD, clearly inside the monsoon flow. On the contrary, for WTB2, the ITD appears as located almost at the station level so that the station can still be submitted to a weak Harmattan flow.

[40] The spatial pattern of surface winds and temperature at Cinzana (Figure 6) confirms the similarities between the weather types indentified in Cinzana and in Banizoumbou.

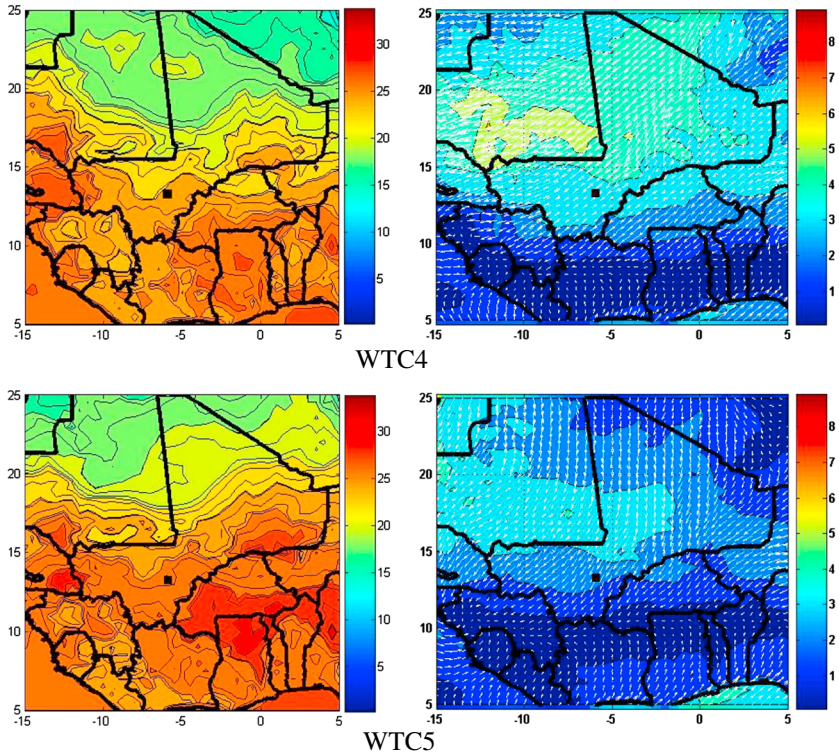

Figure 6. (continued)

At Cinzana, as in Banizoumbou, weather type WTC1 is associated with the highest surface temperature of the five weather types, and the local wind direction is similar to that of Banizoumbou WTB1. Although the local mean wind direction differs from the one recorded in Banizoumbou (E-NE instead of S) (Table 1), the mean mesoscale wind pattern associated with WTC2 is similar (Figure 6) to that of WTC2 and WTC1 (Figure 6). However, for WTC1, the ITD seems to be located at the same latitude as Cinzana or slightly north, while for WTB1, Banizoumbou was clearly located in the monsoon flow. For WTC2 as well as for WTB2, the stations are located on the ITD or slightly south and are submitted to a weak Harmattan flow. The last three weather types (WTC3, WTC4, and WTC5) are characterized by lower mean surface temperatures than for WTC1 and WTC2. They present similar characteristics in terms of surface winds and surface temperature patterns as WTB3, WTB4, and WTB5 in Banizoumbou.

[41] Figures 7 and 8 present the mean vertical profiles of the wind at the two stations for the different weather types. The three Harmattan weather types present a maximum of the zonal wind peaking westward at 925 hPa both in Banizoumbou and Cinzana. This maximum is also evidenced on the meridional wind component for WTB3, WTC5, and WTC4. Even if less intense, this maximum is also obvious in meridional wind for WTC1 and WTC2. It does not appear for WTB1 and is very weak for WTB2. This feature typically reflects the presence of a nocturnal low-level jet (NLLJ). Over the Sahara and the Sahel, the NLLJ is observed both in the dry and wet season, originating either from the northeast during the dry season and from the southwest during the wet season [*Parker et al.*, 2005; *Washington and Todd*, 2005]. Over the Sahel, the wind velocity of the Sahelian NLLJ is maximum at around 05 UTC at 400 m above the ground, with wind speed up to 15 m s^{-1} [*Lothon et al.*, 2008]. The LLJ has been identified as a major meteorological feature for dust emission in the Bodélé Depression (Chad) and more generally over the Sahara [*Schepanski et al.*, 2009]. In our analysis, a strong LLJ appears as associated to the three Harmattan weather types identified at Banizoumbou and Cinzana. The two weather types associated with the monsoon flow do not exhibit such a clear peak in zonal winds at low altitude. WTB2 and WTC2 have a maximum zonal wind component at 850 hPa but exhibit a smoother decrease in wind velocity with height up to 500 hPa (level 5). The mean profile of zonal wind is similar for WTC1, but with lower winds. On the contrary, WTB1 is characterized by relatively high eastward winds above the surface that still may reflect the presence of a LLJ.

[42] All these considerations confirm that similar weather types have been identified in Banizoumbou and Cinzana, particularly during the Harmattan regime.

[43] In the following section, we examine the interannual variability of the weather type decomposition. Owing to the similarity of the weather types in Banizoumbou and Cinzana, we only present the results obtained for Banizoumbou.

4.2. Interannual Variability

[44] The monthly occurrence of the different weather types for the five years studied at Banizoumbou is shown in Figure 9. The main characteristics of the seasonal pattern established from Figure 4 are still visible; however, this time series highlights a significant interannual variability. The weather type distribution can differ from one year to the other, and some anomalies can be distinguished either in the relative occurrence of a given weather type or in terms of change in the timing of the different weather types.

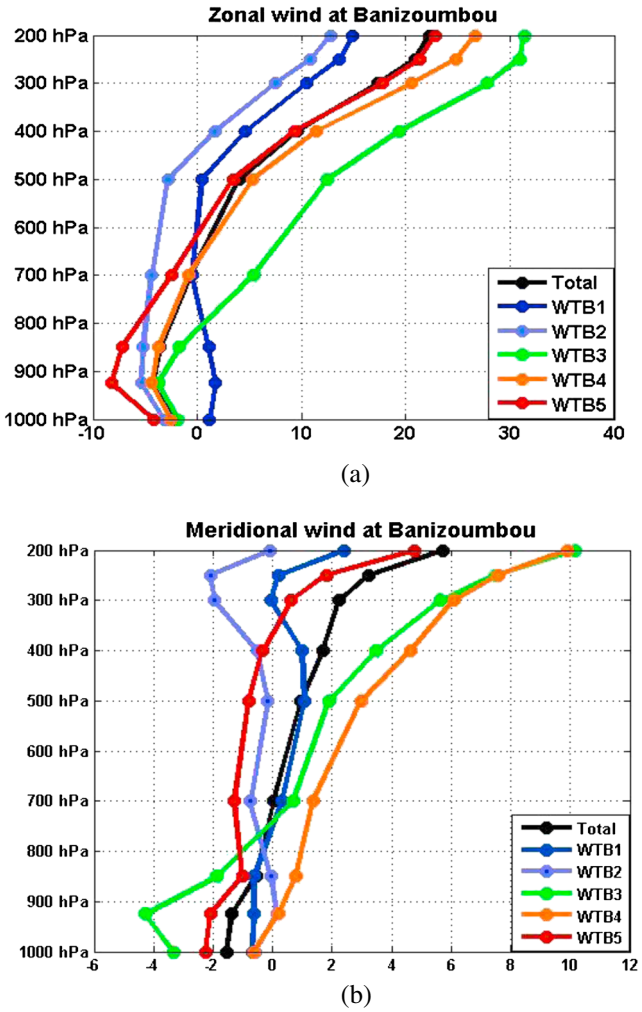

Figure 7. Vertical profiles of the (a) zonal and (b) meridional components of the mean wind for the five weather types at Banizoumbou in m/s.

[45] The time series of the occurrence of the weather type, which has been identified in Banizoumbou, confirms the predominance of a specific weather type at each stage of the dry season, as already shown in Figure 4. However, it also highlights a strong interannual variability in the relative occurrence of the different weather types at some specific time periods.

[46] For the Harmattan weather types, the interannual variability is very high. WTB4 appears as a major weather type from November to February, but with noticeable exceptions. In 2006, Harmattan period is dominated by weather type WTB5 in January, February. In winter 2008–2009, WTB4 only occurs in December with quite short occurrences. During that period, we observe an unusual important WTB3 transition period at the beginning (November) and at the end of winter with important occurrences in February and March and an abrupt switch to WTB1 in April. The winter 2009–2010 is dominated by weather type WTB4 from November to March. For that winter, we observe an important presence of WTB3 in February and March. Quite a strong variability from month to month and from year to year is observed for WTB3 compared to WTB5 and WTB4.

[47] Since the different weather types appear as associated with specific mesoscale meteorological conditions, further investigation on the relation between these mesoscales situations and the synoptic meteorological context should be developed to explain this strong interannual variability in the occurrence of the weather types during the dry season.

5. Relationship Between AOD and PM_{10} Surface Concentration

[48] Since the meteorological situations classified in each weather types have similar characteristics, it is expected that within each weather type, the relationship between surface dust concentration and aerosol optical depth should be less affected by the variability of the atmospheric variables. It might thus be possible to develop a simple method for retrieving dust concentration from AOD for each weather type.

5.1. AOD and PM_{10} Relationship as a Function of Weather Type

[49] For the five years studied, the PM_{10} measurements have been matched with concomitant measured AOD, leading to 2995 synchronous collocated AOD and PM_{10} measurements

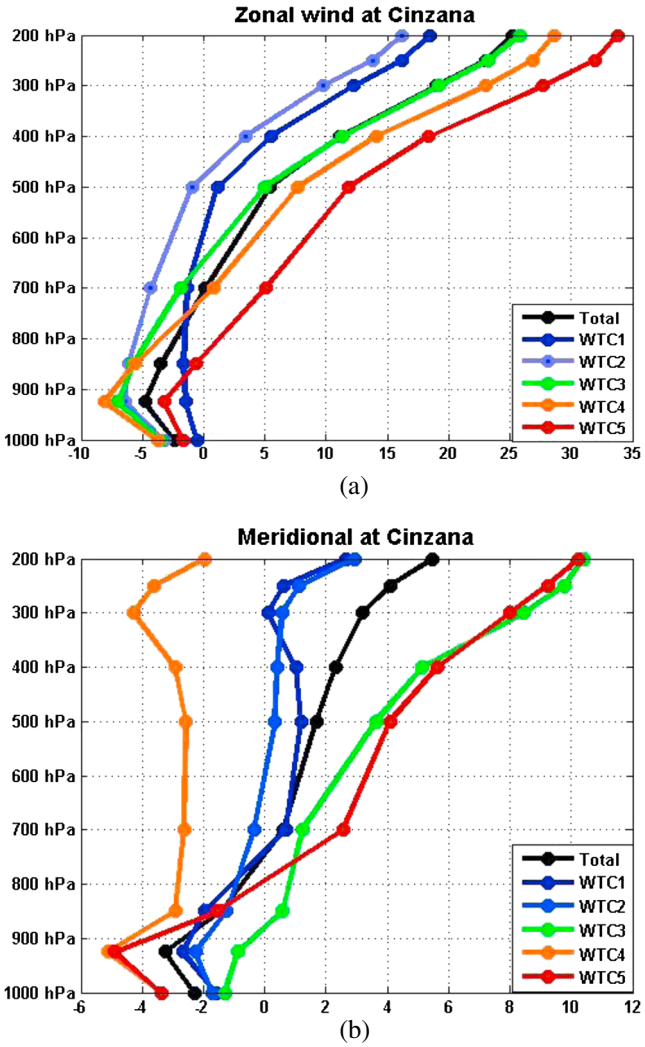

Figure 8. Vertical profiles of the (a) zonal and (b) meridional components of the mean wind for the five weather types at Cinzana in m/s.

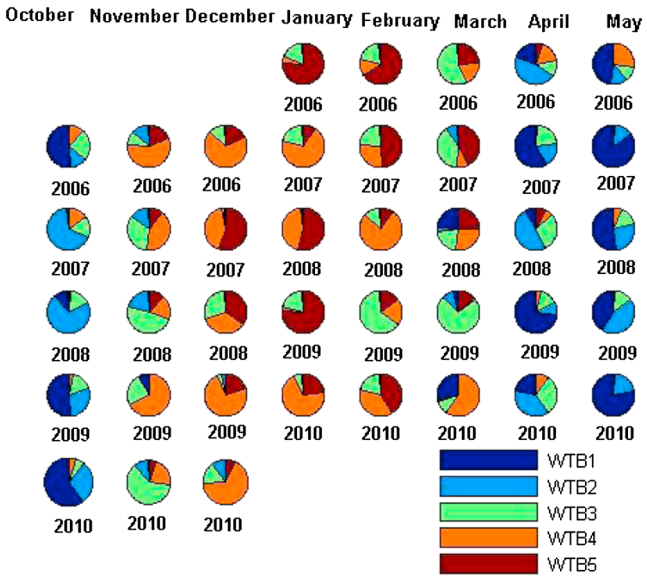

Figure 9. Time series for the five years of study (2006–2010) of the monthly occurrence of the different weather types at Banizoumbou (Niger).

for Banizoumbou and 2294 synchronous collocated measurements for Cinzana. Figures 10 and 11 present the distribution of the PM_{10} and the AOD for the complete data set and for the different weather types.

[50] For the Banizoumbou station (Niger), the hourly PM_{10} concentrations and AOD range over several orders of magnitude (respectively, 2.8 to 461 $\mu g/m^3$ for PM_{10} concentrations and 0.03 to 1.4 for AOD) for the whole data set (Figure 10). This range is not significantly reduced when examining the distribution in the different weather types. Differences appear in the lower quartile (Q25), median, and upper quartile (Q75) values of the distributions.

[51] Considering the PM_{10} concentration, WTB1 is associated with lower median and quartiles Q25 and Q75 (respectively, 66.7, 38.5 and 111 $\mu g/m^3$) than the other WTBs. WTB4 is characterized by the highest median concentration (139 $\mu g/m^3$) and quartile Q75 (>300 $\mu g/m^3$) and tends to have more extreme concentrations than the other WTBs. WTB2, WTB3, and WTB5 have similar median PM_{10} concentrations and comparable quartile Q25 and Q75 values. However, WTB3 shows much lower values (102, 54, and 215 $\mu g/m^3$) than WTB2 and WTB4.

[52] For AOD, WTB4 is associated with lower median and quartiles Q25 and Q 75 (respectively 0.31, 0.18 and 0.60) than the other WTBs. WTB2 is characterized by the highest median values and quartiles Q25 and Q75 (respectively 0.93, 0.41 and 0.60). WTB3 and WTB5 have similar median concentrations and comparable quartile values Q25.

[53] Similar results (Figure 11) are obtained for the Cinzana station (Mali). The hourly PM_{10} concentrations and AOD range over several orders of magnitude (respectively, 3.7 to 422 $\mu g/m^3$ and 0.05 to 1.15) for the whole data set (Figure 11). WTC1 is associated with a lower median and quartiles Q25 and Q75 (respectively, 67.9, 46.8, and 111 $\mu g/m^3$) than the other WTCs. WTC4 is characterized by the highest median concentration (142 $\mu g/m^3$) and quartile Q75 (>256 $\mu g/m^3$) and tends to have much higher concentrations than the other WTCs. However, WTC5 has much lower values (83.2, 52.1, and 150 $\mu g/m^3$) than the WTC2 and WTC3.

[54] For AOD, WTC4 is associated with lower median and quartiles Q25 and Q73 (respectively, 0.32, 0.20, and 0.50) than the other WTCs. WTC1 is characterized by the highest median values and quartile Q25 (respectively, 0.45, 0.32). WTC2 is associated with the highest quartile Q75 (0.74) with respect to the other WTCs.

[55] These results show that the decomposition in weather types does not produce a classification in terms of PM_{10} concentration or AOD range.

[56] For the complete data set, the PM_{10} concentrations have been plotted as a function of AOD in Banizoumbou and Cinzana (Figure 12, upper left panel for each station). Despite a general increasing trend of the PM_{10} concentration with increasing AODs, the regression coefficient, R^2, is relatively low for the two stations ($R^2 = 0.47$ for Banizoumbou, and $R^2 = 0.48$ for Cinzana). It shows that there is no simple significant relationship between the surface dust concentration and the AOD, which represents the vertically integrated dust load.

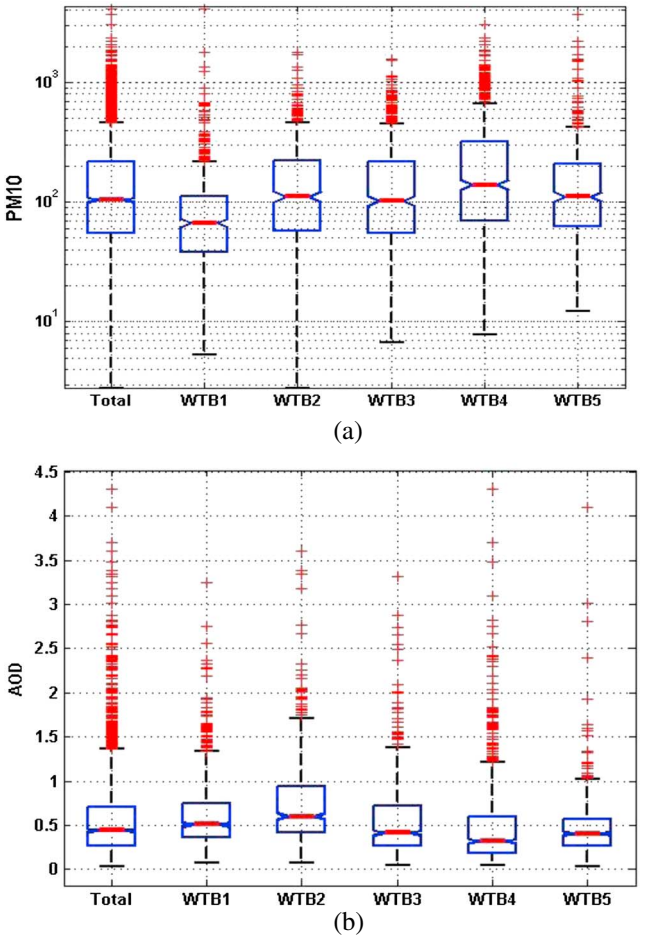

Figure 10. Statistical distribution of (a) PM_{10} ($\mu g/m^3$) and (b) AOD for the complete data set and for the different weather types at Banizoumbou (Niger). The box represents the lower quartile (Q25—lower bar), the median value (middle bar), and the upper quartile (Q75—upper bar) of the studied variable. The T lines delineate the 9th percentile (lower T) and the 91th percentile (upper T) values, respectively.

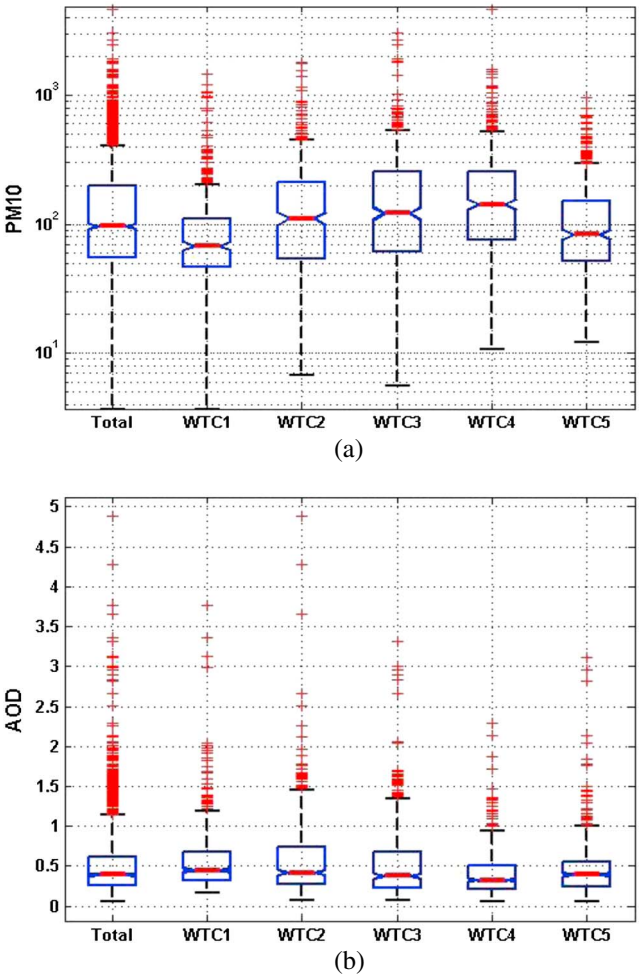

Figure 11. Statistical distribution of (a) PM_{10} ($\mu g/m^3$) and (b) AOD for the complete data set and for the different weather types at Cinzana (Mali). The box represents the lower quartile (Q25—lower bar), the median value (middle bar), and the upper quartile (Q75—upper bar) of the studied variable. The T lines delineate the 9th percentile (lower T) and the 91th percentile (upper T) values, respectively.

[57] The PM_{10} and AOD measurements have been categorized into the five identified weather types. The PM_{10} concentrations have thus been plotted as a function of the AOD for each of the five weather types identified and for the two stations (Figure 12). Except for WTB1 and WTC5, the correlations between the PM_{10} concentrations and the AOD are higher than those obtained for the whole data set. In Banizoumbou, the R^2 coefficients are higher (ranging from 0.58 to 0.79) for the weather types related to the Harmattan regime (WTB3, WBT4, and WTB5) than for those associated with a monsoon flow (R^2 coefficient being, respectively, 0.25 and 0.51 for WTB1 and WTB2). For these two weather types, the PM_{10} distribution (Figure 10) is biased toward low values (less than the median value) while the distribution of the AOD is slightly biased toward high values (higher than the median). This suggests a decorrelation between the PM_{10} concentrations at the ground level and the columnar atmospheric dust load. In this case, the relationship between AOD and PM_{10} is not expected to be linear, and the correlation does not present any statistical significance ($R^2 < 0.4$). The R^2 coefficient is higher for WTB2 than for WTB1, suggesting that the atmospheric column is more homogeneous for the latter weather type. WTB1 corresponds to situations for which the stations are submitted to the monsoon flow. In this case, different aerosol types can be found in the surface monsoon layer and in the elevated Sahara Air layer. This may explain the poor correlation between the surface concentration and the AOD. For the weather types related to the Harmattan, the R^2 correlation coefficients are significant for WTB4 and WTB5 (0.79 and 0.67). The lowest R^2 is obtained for WTB3 ($R^2 = 0.58$).

[58] The same general comments apply to the results obtained at Cinzana. However, the correlation coefficients for the weather types related to the monsoon flow are higher. Weather type WTC5, which represents situations with an important percentage of small PM_{10} concentration values (smaller than 151 $\mu g/m^{-3}$ (Figure 11)), shows a very small linear R^2 correlation coefficient.

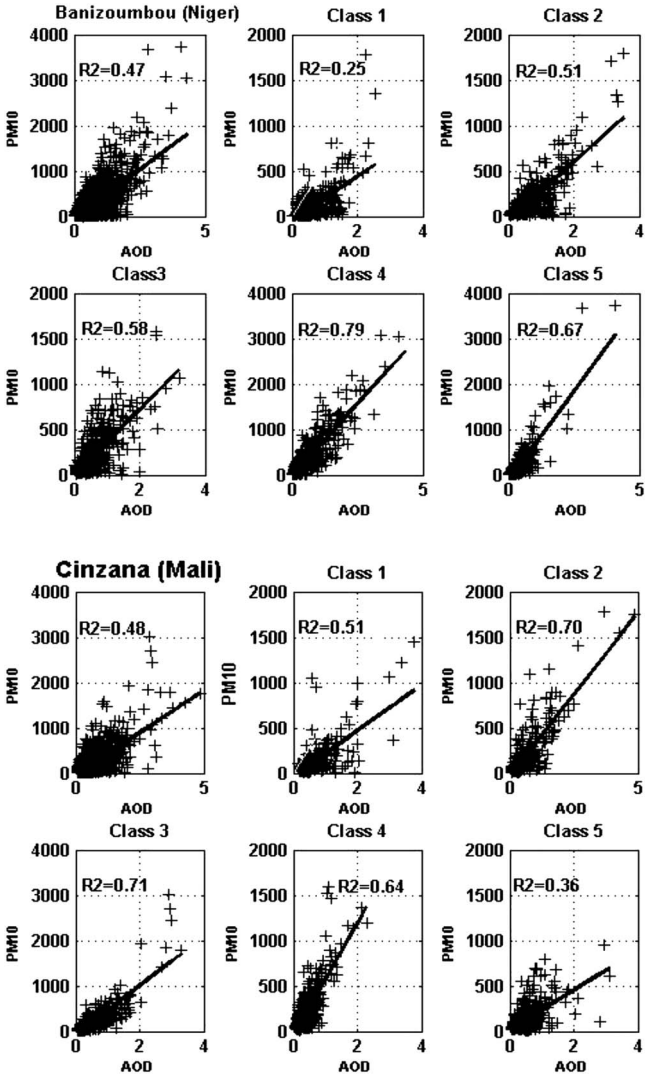

Figure 12. Relationship between the observed particulate matters $(PM_{10})_{Obs}$ ($\mu g/m^3$) and the AOD for the whole studied period (upper left cartoon) and for each weather type at the two stations.

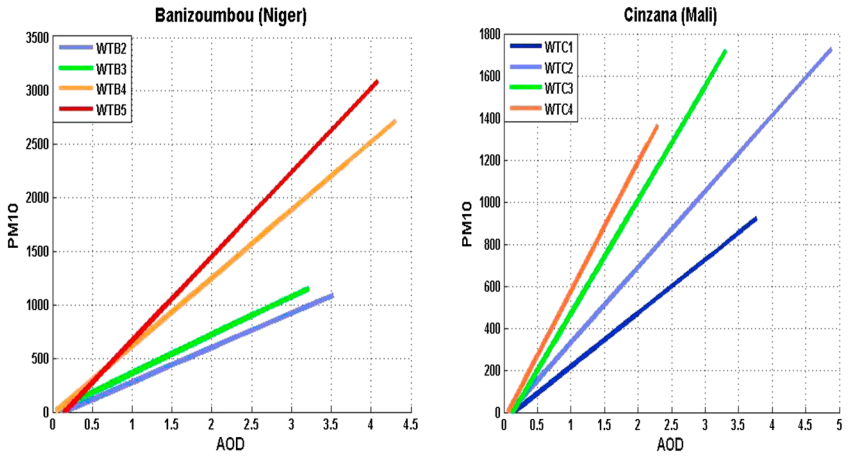

Figure 13. Regression line between AOD and the PM_{10} for each weather type.

[59] These results suggest that, in most of the cases, a specific and significant relationship can be found between the surface PM_{10} concentrations and the AOD when taking into account the differences in the regional meteorological context described by the weather type classification.

[60] The relationships obtained for the different weather types not only differ in terms of correlation but also in terms of the slope of the linear regression. The linear regression obtained for the different weather types in Banizoumbou and Cinzana is plotted in Figure 13. We have excluded the weather types in which the correlation coefficient is lower than 0.5, i.e., corresponding to situations in which the linear regression does not properly represent the relationship between the two measurements (as in WTB1, WTC5). For Banizoumbou, the slope of the regression is significantly higher for WTB5 and WTB4 (respectively, 624 and 737 $\mu g\,m^{-3}$) than for WTB3 and WTB2 (respectively, 385 and 313 $\mu g\,m^{-3}$). Similarly, the two Harmattan weather types identified in Cinzana have higher slopes than the weather types associated with the monsoon flow. These differences imply that for a given measured AOD, the corresponding surface PM_{10} concentration can vary by up to a factor two. As an example, an AOD of 1.5 in Banizoumbou corresponds to a surface concentration of 522 $\mu g/m^3$ in WTB3, slightly lower in WTB2 (414 $\mu g/m^3$), and close to or higher than 1000 $\mu g\,m^{-3}$ in WTB4 and WTB5 (respectively, 899 and 957 $\mu g\,m^{-3}$). In Cinzana, the slope of the regression for the Harmattan weather types ranges from 540 $\mu g\,m^{-3}$ for WTC3 to 700 $\mu g/m^3$ for WTC4. It is close to 360 $\mu g\,m^{-3}$for WTC2 (and for WTB2) and much lower for WTC1 (253 $\mu g/m^3$). These changes in the relationship between the PM_{10} surface concentration and the AOD can reflect differences in the depth of the dust layer in the dust distribution inside the layer. During the dry season, aerosol vertical profiles derived from lidar measurements indicate the persistence of low-level transport for desert dust [*Léon et al.*, 2009; *Cavalieri et al.*, 2010]. The temporal succession of the different weather type during the dry season (WTX2, WTX3, WTX5, WTX4, and WTX1) suggests a progressive increase of the dust concentration at very low altitude from the beginning to the core of the dry season. This can either be due to a decrease in the thickness of the dust layer or to an increase in the dust load. Both phenomena can be related to an intensification of the eastern LLJ, consistent with the vertical profiles of wind velocity (Figures 8 and 9). At the beginning and at the end of the dry season, the surface aerosol layer is thicker, as illustrated by the wind profiles associated with WTC1 and WTX2, which explain the lower slope of the regression for these weather types.

[61] These results show that the surface concentrations cannot be retrieved from the measured AOD without taking the local and regional meteorological context into account. In the following, we thus try to estimate the PM_{10} surface concentration based on the AOD and the local meteorology.

5.2. Statistical Inversion

[62] As the relationship between the PM_{10} and the AOD is not linear, we tried to model it by using dedicated SOM maps. We determined ten different relationships using ten SOM maps denoted $SOM_{i,N}$ ($i = 1,2$ denoting each station, $N = 1\ldots5$ corresponding to each weather type). For each weather type N, the inversion was done by associating AOD and the local meteorology with the corresponding PM_{10} using a

Table 3. Number of Collocated Data for Each Weather Type: (a) Banizoumbou (Niger) Station and (b) Cinzana (Mali) Station

(a)					
Banizoumbou (Niger)	SOM-W1	SOM-W2	SOM-W3	SOM-W4	SOM-W5
Learning set	416	362	456	606	383
Test set	139	120	178	201	127
(b)					
Cinzana (Mali)	SOM-W1	SOM-W2	SOM-W3	SOM-W4	SOM-W5
Learning set	319	423	327	345	309
Test set	106	142	108	114	106

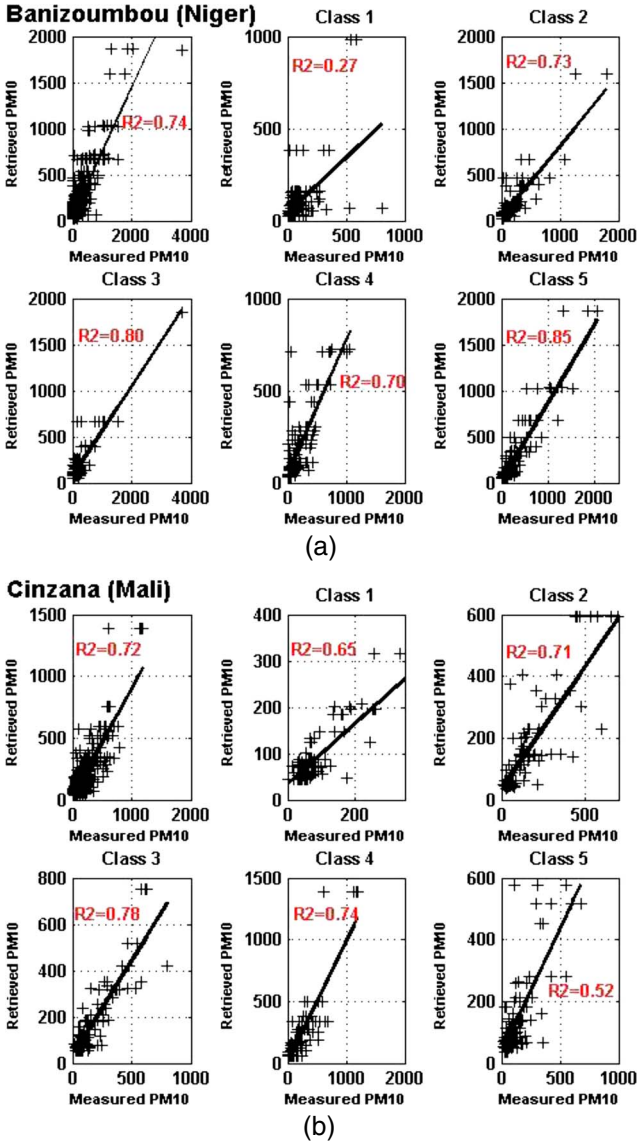

Figure 14. Scatterplot of the PM_{10} retrieval (measured PM_{10} versus retrieved PM_{10} from AOD) for the learning set and the test set for each weather types at the two stations ((a) Banizoumbou and (b) Cinzana) and for aggregating the results of the different classes for the whole studied period.

dedicated $SOM_{i,N}$ map. The inputs of the ten $SOM_{i,N}$ were the AOD measurements at the three selected wavelengths, the meteorological surface parameters from ECMWF at the grid cell containing the station (east-west and north-south components of the wind at surface and the surface temperature) at station *i*. Since each piece of input data (which includes AOD components) is associated with a PM_{10} concentration, each neuron of $SOM_{i,N}$ has captured PM_{10} concentrations and can be characterized by the mean of these captured PM_{10} concentration. Each $SOM_{i,N}$ can thus be considered as modeling the relationship AOD → PM_{10} for a specific weather type at a specific location. In order to have a good accuracy in the PM_{10} retrieval, we used 6 × 6 neuron $SOM_{i,N}$ maps. This number of neurons is a compromise between the number of data we have for obtaining a correct learning procedure (*Kohonen*, 2001) and the accuracy of the relationship we look for.

[63] For each $SOM_{i,N}$, Table 3 shows the number of collocated data pairs (PM_{10} and AOD) used for the learning and the test phases for each weather type for each station.

[64] The PM_{10} concentrations estimated by $SOM_{i,N}$ compared to those measured for each weather type are presented in Figures 14a and 14b for the two sites. The performances of the statistical retrieval for each weather type computed by each $SOM_{i,N}$ at Cinzana and Banizoumbou are shown in the different cartoons of Figure 14; these are satisfactory for most of the weather types. The correlation coefficients between the measured and inverted PM_{10} concentrations range from 0.27 to 0.85. The lowest correlation coefficients are obtained for WTB1 (0.27), WTC1 (0.65), and WTC5 (0.52). For the other weather types, the correlations are higher than 0.7 and higher than those derived from a linear relationship, indicating that the statistical model is able to capture most of the variability of the measured PM_{10} concentrations. The performances of the relationship AOD → PM_{10} computed on the full database (by merging the partial retrievals) are shown in the upper left cartoons of Figures 14a and 14b. The inability of the method to retrieve the PM_{10} concentration from AOD measurements for weather type 1 in Banizoumbou highlights the specific conditions associated with this weather type in this location, for which local meteorological conditions are characteristics of the monsoon flow. This flow can bring other aerosol types (biomass burning, pollution or biogenic aerosols) than dust to the station. In addition, Saharan dust can still be transported from the Sahara but in high layers above the monsoon flow. For weather types WTB2, WTB3, WTB4, and WTB5, the mean transport plays an important role in the aerosol concentration, by advecting aerosols from high dust productive areas such as the Bodélé region. This persistent westward component of the wind favors the homogenization of the aerosol concentration on the atmosphere column, as confirmed by the AOD distribution for WTB2, WTB3, WTB4, and WTB5 (see Figure 10). However, the difference in the slopes of the statistical relationships suggests differences in the thickness of the dust layers during the dry season for the different weather types.

6. Summary and Conclusions

[65] This work investigates the recurrent meteorological situations recorded during the dry season in the Sahel for the period (2006–2010) defined by the so-called weather types and their influence on the relationship between passive remotely sensed measurements of aerosol optical depth and surface dust concentration. During the dry season, surface dust concentrations in the Sahel are mainly related to Saharan dust transport that takes place at low altitude. In such conditions, a simple relationship can be expected between the columnar dust amount and the surface concentration. By modulating the depth and altitude of the dust layers and the intensity of the dust emissions in the source regions, mesoscale meteorological conditions may impact this relationship.

[66] To isolate such influence, we have decomposed the meteorological situations into weather types, each having similar mesoscale characteristics, in terms of wind and temperature profiles at each of the two measurement stations, namely, those in Niger (Banizoumbou) and Mali (Cinzana). To do this, we used a clustering method based on nonlinear artificial neural network, the so-called SOM map, which

was combined with a hierarchical ascendant classification. Five weather types have been identified at each station by processing mesoscale fields of vertical profiles of meridional and zonal winds and temperature, with a specific SOM map at each station, SOM-B and SOM-C. According to the weather type, in situ measurements of mineral dust concentration and aerosol optical depths collected between January 2006 and December 2010 have been processed at the two ground stations, in order to obtain quantitative information on the mineral dust content and its variability over the Sahel.

[67] Three of the five weather types (WTX3, WTX4, and WTX5) identified at the two stations are associated with the Harmattan flux, i.e., the dominant synoptic flow over the region in the dry season. The other two weather types (WTX1 and WTX2) correspond to northward inflows of the monsoon flow at the beginning or at the end of the dry season, (i.e., after the retreat or the installation of the monsoon regime). A general temporal pattern of succession of these weather types can be established along the dry season. After the end of the rainfalls, the WTX2 associated with the monsoon flow occurs mainly in October and November. Then the Harmattan flow becomes well established, and a succession of WTX3, WTX4, and WTX5 is generally observed from November to March. In March and April, the two weather types associated with monsoon flow, and in particular WTX1, prevail. Beside this general pattern, a large interannual variability of the relative occurrence of the different weather types is observed. Further analysis of the synoptic context corresponding to the different weather types should help in understanding this intraseasonal pattern and its interannual variability. In particular, it would be interesting to test the consistency of the identified Harmattan weather types with the synoptic situations associated with the major dust episodes recorded by meteorological stations in March and February between 1983 and 2008 [*Klose et al*., 2010].

[68] For each weather type, we have examined the relationship between the measured AODs and PM_{10} concentrations. The highest surface concentrations and AODs are encountered for the Harmattan weather types. For these weather types, the AODs are significantly correlated with the surface PM_{10} concentrations (except for WTC5), but with large differences in the slope of the regression. These differences in the slope of the regression can be interpreted as changes in the depth of the dust layer during the dry season. As an example, for a given AODs, the corresponding surface concentrations are higher for WTB5 than for WTB3. These results should be confirmed by including in the analysis information on the aerosol vertical profiles during the dry season. This also suggests that the meteorological conditions must be taken into account for retrieving PM_{10} surface concentrations from AODs measurements.

[69] A remote-sensed retrieval of surface PM_{10} concentration has been performed by using a two-step procedure. First, in order to minimize the effect of meteorological variables, which are important, we clustered the meteorological situations in weather types having similar behavior by using SOM-B and SOM-C. Second, for each weather type and at each station, we used dedicated SOM maps (the $SOM_{i,N}$ where i denotes the station, N the weather type given by SOM-B or SOM-C) for retrieving the PM_{10} concentration. The inputs of the $SOM_{i,N}$ are the measured AODs and the local meteorological parameters, and the outputs are the PM_{10} concentration. Except for WTB1 and WTC5, an improved relationship $AOD \rightarrow PM_{10}$ has been found for each WT with respect to linear regressions applied for each weather type. The performances of the inversion computed on the test data sets show a strong improvement for most of the classes, except for WTB1 and WTC5. The good performances of this method should permit the inversion of the mineral dust concentration from AODs derived from satellite observations over the Sahel.

[70] **Acknowledgments.** We warmly thank the local site managers in Niger (Aliko Maman and Alfari Zakou, IRD, Niamey) and Mali (Modibo Coulibaly and Issa Koné, IER, Cinzana) for their efforts in the maintenance of the SDT stations and for providing high-quality data. We thank Didier Tanré for establishing and maintaining the AERONET/PHOTONS site of Banizoumbou, and the AERONET teams for managing the Sun photometer network and data sets. This work was achieved in the frame of the program ADCEM (Impact des Aérosols Désertiques et du Climat sur les Epidémies de Méningites au Sahel) from the French Groupe d'Intérêt Scientifique "Climat-Environnement-Société" (GIS CES) and funded by the ANSES (Agence Nationale de Sécurité Sanitaire de l'Alimentation, de l'Environnement et du Travail). The data from the SDT have been acquired in the Framework of the AMMA (African Monsoon Multidisciplinary Analysis) international program. Based on a French initiative, AMMA was built by an international scientific group and is currently funded by a large number of agencies, especially from France, U.K., U.S., and Africa. It has been the beneficiary of a major financial contribution from the European Community's Sixth Framework Research Programme.

References

Andreae, M. O. (1995), Climatic effects of changing atmospheric aerosol levels, in *World Survey of Climatology: Future Climates of the World*, vol. 16, edited by A. Henderson-Sellers, pp. 341–392, Elsevier, New York.

Andreae, M. O., E. Atlas, H. Cachier, W. R. Cofer III, G. W. Harris, G. Helas, R. Koppmann, J.-P. Lacaux, and D. E. Ward (1996), Trace gas and aerosol emissions from savanna fires, in *Biomass Burning and Global Change*, vol. 1, edited by J. S. Levine, pp. 278–295, MIT Press, Cambridge, Mass.

Brissoli, P., and E. Dittmann (2001), The objective weather type classification of the German Weather Service and its possibilities of application to environmental and meteorological investigations, *Meteorol. Z.*, *10*, 253–260.

Brooks, N., and M. Legrand (2000), Dust variability over northern Africa and rainfall in the Sahel, in *Linking Climate Change to Land Surface Change*, edited by S. J. McLaren and D. Kniveton, pp. 1–25, Kluwer Academic Publishers, New York.

Cavalieri, O., et al. (2010), Variability of aerosol vertical distribution in the Sahel, *Atmos. Chem. Phys. Discuss.*, *10*, 17,609–17,655, doi:10.5194/acpd-10-17609-2010.

De Longueville, F., S. Henry, and P. Ozer (2009), Saharan dust pollution: Implications for the Sahel, *Epidemiology*, *20*(6), 780–934.

Flamant, C., J.-P. Chaboureau, D. J. Parker, C. M. Taylor, J.-P. Cammas, O. Bock, F. Timouk, and J. Pelon (2007), Airborne observations of the impact of a convective system on the planetary boundary layer thermodynamics and aerosol distribution inthe inter-tropical discontinuity région of the West African Monsoon, *Q. J. R. Meteorol. Soc.*, *133*, 1175–1189.

Herman, J. R., P. K. Bhartia, O. Torres, C. Hsu, C. Seftor, and E. Ceralier (1997), Global distribution of absorbing aerosols from Nimbus-7/Toms data, *J. Geophys. Res.*, *102*, 16,911–16,922.

Holben, B. N., et al. (1998), AERONET-A federated instrument network and data archive for aerosol characterisation, *Remote Sens. Environ.*, *66*, 1–16.

Holben, B. N., et al. (2001), An emerging ground-based aerosol climatology: Aerosol optical depth from AERONET, *J. Geophys. Res.*, *106*, 12,067–12,097, doi:10.1029/2001JD900014.

Hsu, C. D., M. A. Whaley, K. Frazer, D. A. Miller, K. A. Mitchell, S. M. Adams, and J. E. O'Tousa (2004), Limited role of developmental programmed cell death pathways in Drosophila norpA retinal degeneration, *J. Neurosci.*, *24*(2), 500–507 (Export to RIS).

Hsu, T.-W., C.-I. Peng, and C.-M. Wang (2006), Austroeupatorium inulifolium (Kunth) King & Robinson (Asteraceae), a newly naturalized plant in Taiwan, *Taiwania*, *51*, 41–45.

Immler, F., and O. Schrems (2002), Determination of tropical cirrus properties by simultaneous LIDAR and radiosonde measurements, *Geophys. Res. Lett.*, *29*(23), 2090, doi:10.1029/2002GL015076.

Jain, A. K., and R. C. Dubes (1988), *Algorithms for Clustering Data*, Prentice Hall, Englewood Cliffs, N. J.

Karyampoudi, V. M., et al. (1999), Validation of the Saharan dust plume conceptual model using lidar meteostat and ECMWF data, *Bull. Am. Meteorol. Soc.*, *80*, 1045–1075.

Klose, M., Y. Shao, M. Karreman, and A. Fink (2010), Sahel dust zone and synoptic background, *Geophys. Res. Let.*, *37*, L09802, doi:10.1029/2010GL042816.

Kohonen, T. (2001), *Self-Organizing Maps*, vol. 501, 3rd ed., pp., Springer-Verlag, Berlin, Heidelberg, New York.

Lavaysse, C., C. Flamant, S. Janicot, and P. Knippertz (2010), Links between African easterly waves, midlatitude circulation and intraseasonal pulsations of the West African heat low, *Q. J. R. Meteorol. Soc.*, *136*(S1), 141–158.

Lebel, T., and A. Ali (2009), Recent trends in the Central and Western Sahel rainfall regime (1990–2007), *J. Hydrol.*, *375*(1–2), 52–64, doi:10.1016/j.jhydrol.2008.11.030.

Legrand, M., A. Plana-Fattori, C. N'Doumé (2001), Satellite detection of dust using the IR imagery of Meteosat, 1. Infrared difference dust index, *J. Geophys. Res.*, *106*, 18,251–18,274.

Léon, J.-F., Y. Derimian, I. Chiapello, D. Tanré, T. Podvin, B. Chatenet, A. Diallo, and C. Deroo (2009), Aerosol vertical distribution and optical properties over M'Bour (16.96_W; 14.39_ N), Senegal from 2006 to 2008, *Atmos. Chem. Phys.*, *9*, 9249–9261.

Lothon, M., F. Said, F. Lohou, and B. Campistron (2008), Observation of the diurnal cycle in the low troposphere of West Africa, *Mon. Weather Rev.*, *136*(9), 3477–3500, doi:10.1175/2008MWR2427.1.

Marticorena, B., B. Chatenet, J. L. Rajot, S. Traoré, M. Coulibaly, A. Diallo, I. Kon´e, A. Maman, T. N'Diaye, and A. Zakou (2010), Temporal variability of mineral dust concentrations over West Africa: Analyses of a pluriannual monitoring from the AMMA Sahelian Dust Transect, *Atmos. Chem. Phys. Discuss.*, *10*, 8051–8101, doi:10.5194/acpd-10-8051-2010.

Mathon, V., H. Laurent, and T. Lebel (2002), Mesoscale convective system rainfall in the Sahel, *J. Appl. Meteorol.*, *41*, 1081–1092, doi:10.1175/1520-50(2002)041<1081:MCSRIT>2.0.CO;2.

N'Tchayi Mbourou, G. M., J. Bertrand, M. Legrand, and J. Baudet (1994), Temporal and spatial variations of the atmospheric dust loading throughout West Africa over the last thirty years, *Ann. Geophys.*, *12*, 265–273.

Ogunjobi, K. O., Z. He, and C. Simmer (2008), Spectral aerosol optical properties from AERONET Sun-photometric measurements over West Africa, *Atmos. Res.*, *88*, 89–107.

Parker, D. J., R. R. Burton, A. Diongue-Niang, R. J. Ellis, M. Felton, C. M. Taylor, C. D. Thorncroft, P. Bessemoulin, and A. M. Tompkins (2005), The diurnal cycle of the West African monsoon circulation, *Q. J. R. Meteorol. Soc.*, *131*, 2839–2860, doi:10.1256/qj.04.52.

Pauley, P. M., N. L. Baker, and E. H. Barker (1996), An observational study of the "Interstate 5" dust storm case, *Bull. Am. Meteorol. Soc.*, *77*, 693–720.

Prospero, J. M., and T. N. Carlson (1972), Vertical and areal distribution of Saharan dust over the western equatorial North Atlantic Ocean, *J. Geophys. Res.*, *77*, 5255–5265.

Prospero, J. M., and R. T. Nees (1977), Dust concentration in the atmosphere of the Equatorial.

Prospero, J. M., P. Ginoux, O. Torres, S. E. Nicholson, and T. E. Gill (2002), Environmental characterization of global sources of atmospheric soil dust identified with the Nimbus 7 Total Ozone Mapping Spectrometer (TOMS) absorbing aerosol product, *Rev. Geophys.*, *40*(1), 1002, doi:10.1029/2000RG000095.

Ramanathan, V., et al. (2001), The Indian Ocean Experiment: Widespread haze from south and southeast Asia and its climate forcing, *J. Geophys. Res.*, *106*, 28,371–28,398.

Saporta, G. (1990), Probabilités, analyses de données et statistique, Ed. Technip-Paris.

Schepanski, K., I. Tegen, M. C. Todd, B. Heinold, G. Bönisch, B. Laurent, and A. Macke (2009), Meteorological processes forcing Saharan dust emission inferred from MSG-SEVIRI observations of subdaily dust source activation and numerical models, *J. Geophys. Res.*, *114*, D10201, doi:10.1029/2008JD010325.

Shi, Y., J. Zhang, J. S. Reid, B. Holben, E. J. Hyer, and C. Curtis (2011), An analysis of the collection 5 MODIS over-ocean aerosol optical depth product for its implication in aerosol assimilation, *Atmos. Chem. Phys.*, *11*, 557–565, doi:10.5194/acp-11-557.

Thomson, M. C., A. M. Molesworth, M. H. Djingarey, K. R. Yameogo, F. Belanger, and L. E. Cuevas (2006), Potential of environmental models to predict meningitis epidemics in Africa, *Trop. Med. Int. Health*, *11*(6), 781–788.

Torres, O., P. K. Bhartia, J. R. Herman, Z. Ahmad, and J. Gleason (1998), Derivation of aerosol properties from satellite measurements of backscattered ultraviolet radiation: Theoretical basis, *J. Geophys. Res.*, *103*, 17,099–17,110.

Vautard, R. (1990), Multiple weather regimes over the north Atlantic: Analysis of precursors and successors, *Mon. Weather Rev.*, *118*, 2056–2081.

Washington, R., and M. C. Todd (2005), Atmospheric controls on mineral dust emission from the Bode´le´ Depression, Chad: The role of the low level jet, *Geophys. Res. Lett.*, *32*, L17701, doi:10.1029/2005GL023597.

Washington, R., et al. (2006), Links between topography, wind, deflation, lakes and dust: The case of the Bodele depression, Chad, *Geophys. Res. Lett.*, *33*, L09401, doi:10.1029/2006GL025827.

Yahi, H., R. Santer, R. A. Weill, A. M. Crepon, and S. Thiria (2011), Exploratory study for estimating atmospheric low level particle pollution based on vertical integrated optical measurements, *Atmos. Environ.*, *45*, 3891–3902, doi:10.1016/j.atmosenv.2010.11.047.